Asian Journal of Chemistry; Vol. 38, No. 6 (2026), 1403-1410
ASIAN JOURNAL OF CHEMISTRY
https://doi.org/10.14233/ajchem.2026.35664

Plant-Assisted Synthesis of Mesoporous CuO Nanoparticles from *Sesbania aculeata* and their Application in Degradation of Malachite Green Dye

ANUSHA RACHAPUDI, BUDATI BALA VENKATA SAILAJA*, ATHOTA CHANDRA LEELA, SANDHYA RANI NAYAK, LOKESH MUDARAPU and AMBIKA MANCHA

Department of Chemistry, Andhra University, Visakhapatnam-530003, India

*Corresponding author: E-mail: dr.bbvsailaja@andhrauniversity.edu.in

Received: 28 January 2026 *Accepted*: 10 April 2026 *Published online*: 31 May 2026 AJC-22366

In this study, CuO NPs were prepared through a sustainable green synthesis approach employing *Sesbania aculeata* (Dhaincha) leaf extract. The phytochemical-rich extract served a dual role by facilitating the reduction of copper ions and stabilizing the formed nanoparticles, eliminating the need for external chemical reagents. The synthesised CuO NPs were investigated using XRD, UV-Vis DRS, FTIR, FESEM-EDS, TGA and BET analyses. XRD confirmed the formation of crystalline monoclinic CuO NPs with an average crystallite size of 22.6 nm. UV-Vis DRS revealed a band gap energy of 2.7 eV, confirming the successful formation of CuO NPs. FTIR spectra indicated the effective involvement of plant-derived phytochemicals in capping and stabilizing the nanoparticle surface. TGA demonstrated minimal mass loss beyond 400 ºC, demonstrating high thermal stability and purity of the synthesised CuO NPs. BET surface area revealed a characteristic Type-IV nitrogen adsorption–desorption isotherm accompanied by a well-defined hysteresis loop, confirming the mesoporous nature of the material with a specific surface area of 89.7 $m^2 g^{-1}$. Furthermore, the green-synthesised CuO NPs showed efficient photocatalytic degradation of malachite green dye within 100 min. This study highlights the potential of *S. aculeata*-mediated CuO nanoparticles as sustainable, multifunctional nanomaterials for environmental remediation and biomedical applications.

Keywords: Green synthesis, *Sesbania aculeata*, CuO NPs, Photocatalytic degradation.

INTRODUCTION

Nanotechnology focuses on the design and manipulation of materials at the nanoscale, where unique physico-chemical properties enable diverse applications [1]. Nanoparticles are commonly synthesised using physical and chemical methods [2], but concerns regarding toxicity, cost and environmental impact have encouraged the development of safer alternatives. Their small size and enhanced reactivity have led to widespread applications in pharmaceuticals, electronics, textiles and environmental systems [3,4], although understanding nanoparticle-biological interactions remains essential to address potential nanotoxicological risks [5].

Green synthesis using plant resources has emerged as an eco-friendly and sustainable strategy for nanoparticle production [6]. Plant extracts contain bioactive phytochemicals that act as natural reducing and stabilising agents, enabling controlled synthesis without the use of hazardous chemicals [7]. Such plant-mediated nanoparticles generally exhibit lower toxicity and improved compatibility for biological and environmental applications [8-10].

Metal and metal oxide nanoparticles have gained considerable attention due to their functional versatility in catalysis and environmental remediation [11,12]. Among these, copper-based nanoparticles are particularly attractive owing to their cost-effectiveness and significant catalytic and redox properties [13-15]. Their ability to participate in reactive oxygen species (ROS)-related processes further supports their potential in environmental and biological systems [16]. In this study, copper oxide (CuO) nanoparticles were synthesised using *Sesbania aculeata* (Dhaincha) leaf extract as a green reducing and stabilising agent. *S. aculeata* is a phytochemically rich plant containing flavonoids, phenolics, alkaloids and other bioactive compounds that facilitate metal ion reduction and nanoparticle stabilisation. The functional groups present in these metabolites play a key role in controlling nucleation and growth, eliminating the need for external reagents. Despite extensive reports on plant-mediated nanoparticle synthesis,

the use of *S. aculeata* for CuO NPs fabrication remains largely unexplored, highlighting the novelty of this approach.

The synthesised CuO nanoparticles were characterised using UV-Vis, FTIR, PXRD, FESEM-EDS, N_2 adsorption–desorption and thermogravimetric analysis. Their photocatalytic efficiency was evaluated through the degradation of malachite green dye, demonstrating their potential for environmental remediation applications.

EXPERIMENTAL

Copper(II) nitrate trihydrate [$Cu(NO_3)_2 \cdot 3H_2O$] was used as copper precursor and sodium hydroxide served for pH adjustment during synthesis. Ethanol was employed as the washing solvent to remove residual organic matter. Malachite green dye was selected for photocatalytic degradation studies. All chemicals were of analytical grade, sourced from reputed suppliers including Sigma-Aldrich and Coastal Chemicals and used without further purification. Double-distilled water was used throughout and all glassware was thoroughly cleaned, rinsed and oven-dried prior to use.

Preparation of leaf extract: Fresh leaves of *Sesbania aculeata* (Dhaincha) were collected from agricultural fields in Kothapeta village (16.716015º N, 81.895782º E) of Andhra Pradesh state, India and authenticated by qualified taxonomist. The collected leaves were thoroughly washed with tap water, followed by double-distilled water, to remove surface dust and extraneous impurities. The cleaned leaves were shade-dried under ambient conditions (25-30 ºC) for 7-10 days until a constant weight was attained. The dried material was pulverised into a fine powder using a clean electric grinder and subsequently sieved through a 60-mesh screen to ensure uniform particle size. For aqueous extract preparation, 10 g of leaf powder was mixed with 100 mL of distilled water and heated at 60-70 ºC for 20 min. The mixture was then cooled to room temperature and filtered using Whatman No. 1 filter paper to obtain a clear extract. The filtrate was further centrifuged at 15,000 rpm for 10 min and the resulting supernatant was stored at 4 ºC for subsequent use and characterisation.

Analysis of phytochemicals: The prepared leaf extract was subjected to qualitative phytochemical screening to determine the presence of key secondary metabolites. The screening involved standard tests for flavonoids (Shinoda test), alkaloids (Hager's test), tannins (gelatin test), saponins (Froth test), phenolic compounds (ferric chloride test), glycosides (Keller-Killiani test) and terpenoids (Salkowski test). All analyses were carried out following established phytochemical protocols reported in the literature [17,18].

Flavonoid detection test

Shinoda test: When 1 mL of *S. aculeata* leaf extract was treated with magnesium turnings and a few drops of conc. HCl, a pink to red colour developed, indicating the presence of flavonoids.

Phenolic compounds detection test ($FeCl_3$ test): On adding a few drops of 5% $FeCl_3$ to 1 mL of extract, a bluish-green colour appeared, indicating the presence of phenolic compounds.

Tannins detection test (gelatin test): Mixing 1 mL of extract with 1 mL of 1% gelatin solution containing NaCl led to the formation of a dark precipitate, confirming tannins.

Alkaloids detection test (Hager's test): The addition of Hager's reagent to 1 mL of extract resulted in a yellow precipitate, which indicated the presence of alkaloids.

Saponins detection test (Froth test): When 1 mL of extract was vigorously shaken with 2 mL of distilled water, a stable froth persisted, confirming the presence of saponins.

Terpenoids detection test (Salkowski test): Treating 1 mL of extract with 2 mL of chloroform followed by careful addition of conc. H_2SO_4 produced a reddish-brown interface, indicating terpenoids.

Glycosides detection test (Keller-Killiani test): Upon adding glacial acetic acid containing a trace of $FeCl_3$ to 1 mL of extract and then carefully introducing conc. H_2SO_4, a brown ring formed at the interface, confirming glycosides.

Synthesis of CuO NPs: CuO NPs were synthesised *via* a green precipitation approach. For fabrication of CuO NPs, 50 mL of 0.1 M $Cu(NO_3)_2 \cdot 3H_2O$ solution was combined with an equal volume (50 mL) of the prepared leaf extract under continuous magnetic stirring at 70 ºC for 2 h. The pH of the reaction mixture was gradually adjusted to approximately 10 by the dropwise addition of 1 M NaOH, resulting in the appearance of a dark brown to black precipitate, signifying the formation of CuO NPs. The reaction mixture was allowed to age for 2 h to ensure complete precipitation. The resulting solid was separated by centrifugation at 6000 rpm for 10 min and repeatedly washed with distilled water followed by ethanol to remove residual impurities and surface-bound organic species. The obtained material was dried at 80 ºC for 12 h and subsequently calcined in a muffle furnace at 400 ºC for 3 h to yield crystalline CuO NPs. The yield percentage of CuO NPs was determined using the following formula:

$$\text{Yield (\%)} = \frac{\text{Experimental weight of CuO}}{\text{Theoretical weight of CuO}} \times 100$$

Characterisation of CuO NPs: The optical absorption characteristics of the synthesised CuO NPs were examined using a Cary 60 UV-visible spectrophotometer, while their thermal stability and mass variation were evaluated by thermogravimetric analysis (TGA) on a Hitachi STA 7300 from room temperature to 1000 ºC. Fourier transform infrared (FTIR) spectra were recorded using a Bruker Alpha-II spectrophotometer in the 4000-500 cm^{-1} range to identify functional groups involved in nanoparticle formation. The surface area and pore characteristics were determined by Brunauer-Emmett-Teller (BET) analysis based on N_2 adsorption–desorption isotherms at 77 K using a Quantachrome NOVA Touch 4 LX instrument. The crystalline structure of the CuO nanoparticles was analysed by powder X-ray diffraction employing a Bruker D8 advance diffractometer, while surface morphology and elemental composition were examined using a scanning electron microscope (SEM, Carl Zeiss Supra 40, Germany) equipped with energy-dispersive X-ray analysis (EDAX), confirming the formation of phase-pure CuO NPs.

RESULTS AND DISCUSSION

Qualitative phytochemical screening plays a critical role in green nanoparticle synthesis by identifying bioactive constituents that function as reducing, capping and stabilising agents. These phytochemicals such as flavonoids, phenolics, alkaloids and terpenoids facilitate the reduction of metal ions, regulate nucleation and growth kinetics and enhance colloidal stability through surface functionalisation. Thus, phytochemical profiling provides a direct basis for correlating plant-derived metabolites with nanoparticle formation mechanisms and their resulting physico-chemical and functional properties. The analysis of *S. aculeata* leaf extract confirmed the presence of these key bioactive constituents as summarised in Table-1.

XRD studies: X-ray diffraction was used to analyze the crystalline structure of the green-synthesised CuO NPs (Fig. 1). Diffraction peaks observed at 2θ = 32.63º, 35.66º, 38.78º, 48.93º, 53.61º, 58.19º, 61.54º, 66.06º, 68.18º and 75.07º correspond to the (110), $(\bar{1}11)$, (111), $(\bar{2}02)$, (020), (202), $(\bar{1}13)$, $(\bar{3}11)$, (220) and (004) planes of monoclinic CuO. These peaks match well with JCPDS card No. 89-5899, confirming phase-pure CuO NPs formation [19]. The absence of impurity peaks indicates high phase purity, while the sharp reflections demonstrate good crystallinity. The average crystallite size (D) calculated using the Debye-Scherrer equation:

$$D = \frac{k\lambda}{\beta \cos\theta} \quad (2)$$

where K is the shape factor (taken as 0.9), λ denotes the wavelength of Cu*K*α radiation (1.5406 Å), β corresponds to the full width at half maximum (FWHM) of the diffraction peak and θ is the Bragg diffraction angle. The average crystallite size of the CuO NPs was estimated to be approximately 22.6 nm. This nanoscale dimension confirms the successful formation of well-crystallised nanostructured CuO NPs.

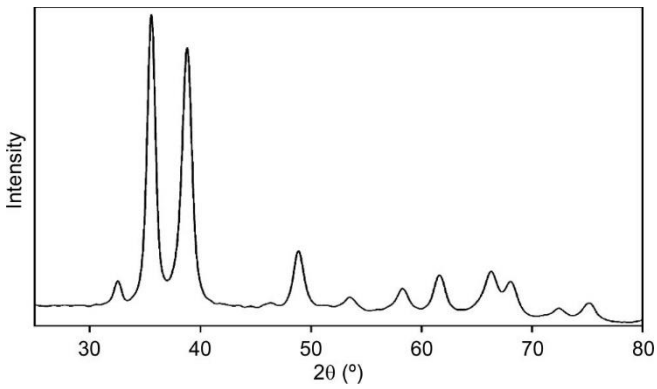

Fig. 1. X-ray diffraction spectrum of biosynthesised CuO nanoparticles

FT-IR studies: The FTIR spectrum confirms the formation of green-synthesised CuO NPs and the role of phytochemicals in their stabilisation [20]. The broad band around 3400 cm^{-1} is attributed to –OH stretching vibrations of phenolic and flavonoid compounds, indicating their involvement in reduction and capping. The weak absorption near 2920 cm^{-1} corresponds to aliphatic C–H stretching of plant-derived organic residues. The band observed at 1630 cm^{-1} is assigned to C=O stretching or H–O–H bending vibrations of adsorbed biomolecules. Peaks in the 1050–1150 cm^{-1} region arise from C–O stretching of polyphenols. A strong absorption band below 600 cm^{-1}, particularly around 530 cm^{-1}, is characteristic of Cu–O stretching vibrations, confirming the formation of CuO NPs (Fig. 2).

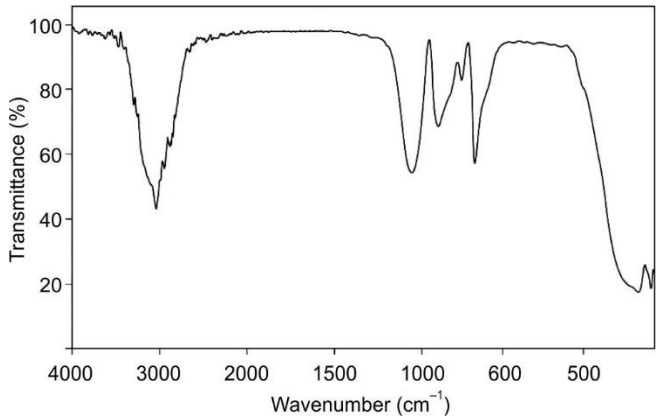

Fig. 2. FTIR spectrum of the green-fabricated CuO nanoparticles

SEM-EDS studies: SEM images of the biosynthesised CuO NPs (Fig. 3) show agglomerated, irregularly shaped nanograins with a rough surface morphology [21]. The observed agglomeration is attributed to high surface energy and phytochemical-assisted stabilisation during the green synthesis process, which promotes particle clustering while restricting excessive growth. Such surface features are beneficial for surface dependent applications [22]. The accompanying EDS spectrum displays distinct signals corresponding only to copper and oxygen, confirming the successful formation of CuO NPs. The absence of peaks from other elements verifies the high purity of the synthesised material.

Thermal studies: Thermogravimetric analysis was performed over 30-1000 ºC at a heating rate of 10 ºC min^{-1} to

TABLE-1
QUALITATIVE ASSESSMENT OF PHYTOCONSTITUENTS IN *Sesbania aculeata* LEAVES

Phytochemical	Test performed	Observation	Inference
Flavonoids	Shinoda test	Pink/red colour development	Flavonoids present
Phenolic compounds	Ferric chloride test	Bluish-green colour formation	Phenolic compounds present
Tannins	Gelatin test	Dark precipitate formation	Tannins present
Alkaloids	Hager's test	Yellow precipitate observed	Alkaloids present
Saponins	Froth test	Stable persistent froth	Saponins present
Terpenoids	Salkowski test	Reddish-brown interface	Terpenoids present
Glycosides	Keller–Killiani test	Brown ring at the interface	Glycosides present

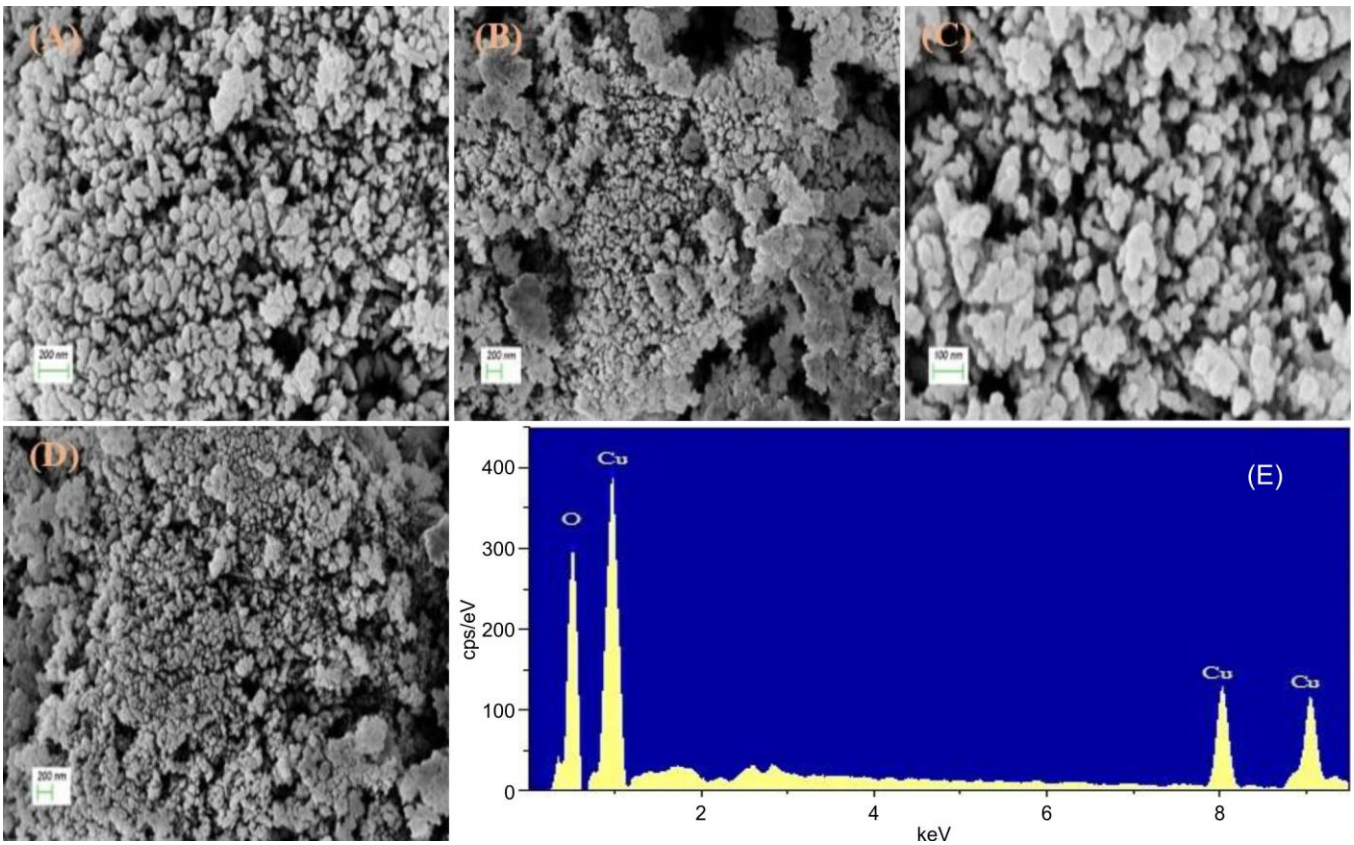

Fig. 3. (A-D) FESEM images, (E) EDS spectrum of CuO NPs

evaluate the thermal stability and purity of the green synthesised CuO NPs [23,24]. An initial weight loss of 19.65% between 63 ºC and 125 ºC is attributed to the removal of physically adsorbed moisture and loosely bound surface species (Fig. 4). A second weight loss of 27.7% in the range of 125-369 ºC corresponds to the decomposition of residual organic constituents and phytochemicals from the plant extract. Beyond 400 ºC, negligible mass change is observed, indicating the complete removal of organic residues and the formation of stable CuO. The absence of further decomposition at higher temperatures confirms the thermal stability and compositional purity of the synthesised nanoparticles, supporting their applicability under elevated temperature conditions.

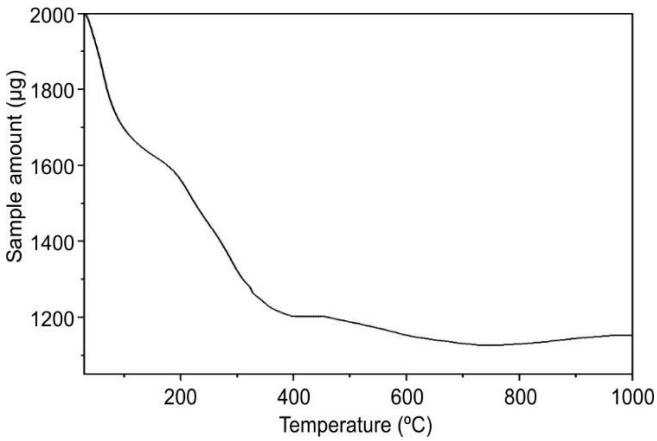

Fig. 4. Thermogram of the CuO NPs

Brunauer-Emmett-Teller (BET): The N_2 adsorption–desorption profile of the biosynthesised CuO NPs displays a typical Type-IV isotherm accompanied by a well-defined hysteresis loop, confirming the presence of a mesoporous architecture [25,26] (Fig. 5a). At lower relative pressures ($P/P_o < 0.3$), nitrogen uptake increases gradually, corresponding to surface adsorption and the formation of a monolayer. A pronounced rise in adsorption is observed in the intermediate pressure range ($P/P_o \approx 0.6$-0.9), which can be attributed to capillary condensation occurring within the mesoporous network. The N_2 adsorption–desorption isotherm shows a distinct hysteresis between adsorption and desorption branches, indicating interconnected pores with irregular geometry. As the relative pressure approaches saturation ($P/P_0 \approx 1.0$), the adsorption curve reaches a plateau, confirming complete pore filling. The CuO NPs exhibit a high specific surface area of 89.7 $m^2\ g^{-1}$, an average pore diameter of 21 nm and a pore volume of 0.13 $cm^3\ g^{-1}$, demonstrating a well-developed mesoporous structure (Table-2). The sharp peak in the BJH pore size distribution further confirms uniform mesopore formation (Fig. 5b). These structural features provide a large number of accessible active sites, enhancing the photocatalytic efficiency of the material.

UV-Visible spectral studies: The UV-Vis absorption spectrum of CuO NPs is presented in Fig. 6. Two absorption bands were observed, with an intense peak around 223 nm and a weaker band near 345 nm. The strong absorption in the deep UV region is attributed to charge-transfer transitions between O^{2-} and Cu^{2+} ions, confirming the formation of CuO

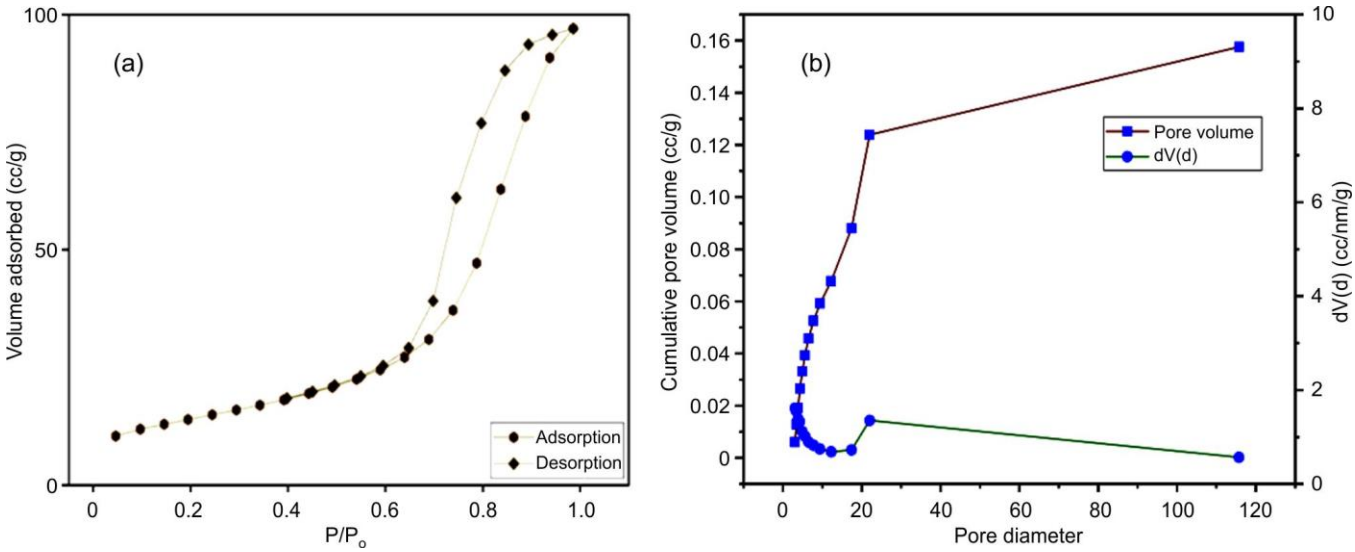

Fig. 5. (a) BET nitrogen adsorption–desorption isotherm of biosynthesised CuO nanoparticles, (b) pore size distribution

TABLE-2
BET SURFACE AREA, PORE SIZE AND VOLUME OF CuO NANOPARTICLES

BET surface area (m^2/g)	Pore diameter (nm)	Pore volume (cc/g)	Isotherm (IUPAC)	Relative pressure (P/P_o)	BET constant
89.7	21	0.13	Type-IV	0.33	98.54

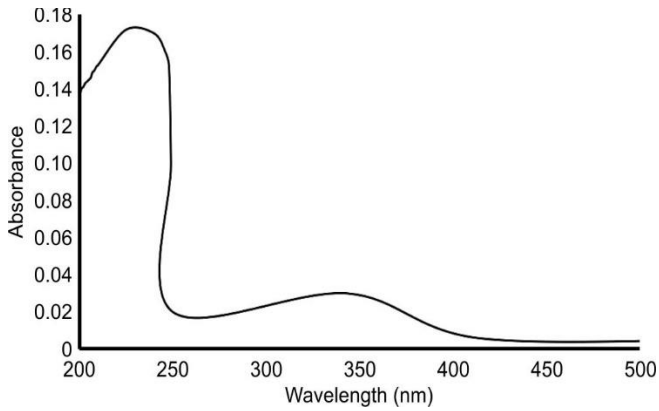

Fig. 6. Optical absorption spectrum of the green-synthesised CuO nanoparticles

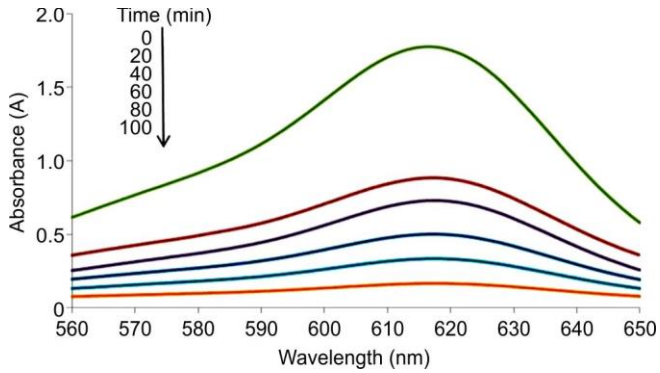

Fig. 7. Photocatalytic degradation of malachite green

nanoparticles. The broader band at ~345 nm is associated with surface defect states and size-dependent electronic transitions typical of nanoscale CuO systems. The optical band gap, estimated from the Tauc plot, was found to be approximately 2.7 eV [27,28]. This slight increase compared to bulk CuO can be attributed to quantum confinement effects and surface modification by phytochemicals involved in the green synthesis process.

Degradation of malachite green dye: The UV-Vis absorption spectra demonstrate the progressive photocatalytic degradation of the dye in the presence of green-synthesised CuO NPs under visible light irradiation. The untreated dye shows a distinct absorption maximum at ~620 nm, corresponding to π-π transitions of the conjugated chromophore. With increasing irradiation time (0-100 min), a continuous decrease in absorbance intensity is observed, indicating effective degradation of the dye, reaching approximately 98% removal within 100 min (Fig. 7).

$$\text{Degradation (\%)} = \frac{C_o - C_t}{C_o} \times 100 \quad (3)$$

where C_o indicates initial absorbance and its absorbance at a certain time t is C_t.

The continuous decrease in absorbance intensity without the appearance of new peaks indicates that the process is governed by photocatalytic degradation rather than simple adsorption. The absence of any significant wavelength shift suggests that no stable coloured intermediates are formed, implying direct breakdown of the chromophoric structure into smaller, colourless products such as CO_2, H_2O and inorganic ions. The enhanced photocatalytic performance of the green-synthesised CuO NPs is attributed to their nanoscale dimensions, which promote efficient generation and separation of charge carriers, thereby reducing electron–hole recombination. In addition, the mesoporous structure and high surface area provide abundant active sites for adsorption and interfacial redox reactions, improving catalytic efficiency.

TABLE-3
COMPARATIVE EVALUATION OF PHOTOCATALYTIC PERFORMANCE OF CuO NANOPARTICLES

Plant used	Dye	Degradation (%)	Degradation time	Ref.
Musa paradisiaca	Malachite green	94.41	4 h	[29]
Aloe barbadensis	Malachite green	70.00	120 min	[30]
Mangifera Indica	Malachite green	95.39	–	[31]
Sesbania aculeata	Malachite green	98.00	100 min	Present study

A comparative analysis (Table-3) shows that the present system achieves 98% degradation of malachite green within 100 min, outperforming previously reported systems such as *Musa paradisiaca* (94.41% in 4 h) and *Aloe barbadensis* (70% in 120 min), indicating a faster and more efficient photocatalytic process.

Effect of pH: The influence of pH on photocatalytic degradation is illustrated in Fig. 8a. Under acidic conditions (pH 3 and 5), the degradation efficiency remains low, likely due to weaker interaction between dye molecules and the catalyst surface. As the pH increases, the degradation efficiency improves and reaches a maximum at pH 10, as reflected by the rapid decrease in C/C_o. This enhanced performance in alkaline conditions is attributed to increased generation of reactive hydroxyl radicals ($^{\bullet}OH$), which accelerate dye degradation. A slight decrease at pH 12 may result from excess ^{-}OH ions promoting charge recombination or modifying the catalyst surface. The corresponding degradation percentages at different pH values are shown in Fig. 8b, with pH 10 identified as the optimal condition for photocatalytic activity.

Effect of dye: The effect of initial dye concentration on photocatalytic activity is shown in Fig. 9a. As the concentration increases from 5 to 15 ppm, a more significant decrease in C/C_0 is observed, indicating effective utilisation of active

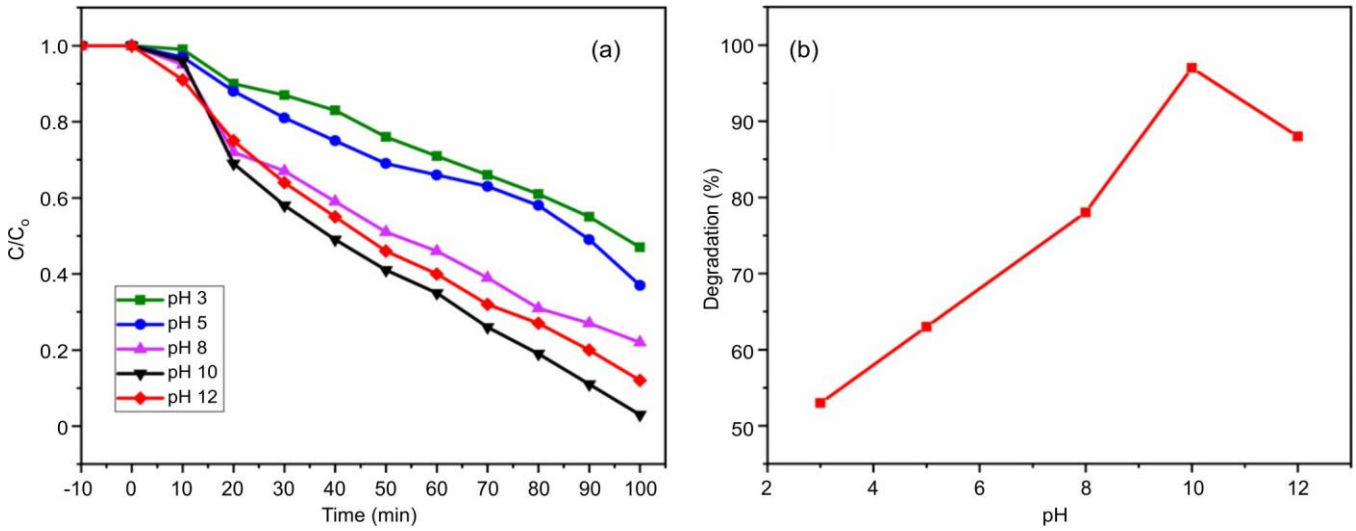

Fig. 8. (a) Effect of pH on the removal of MG dye, (b) % degradation at different pH values

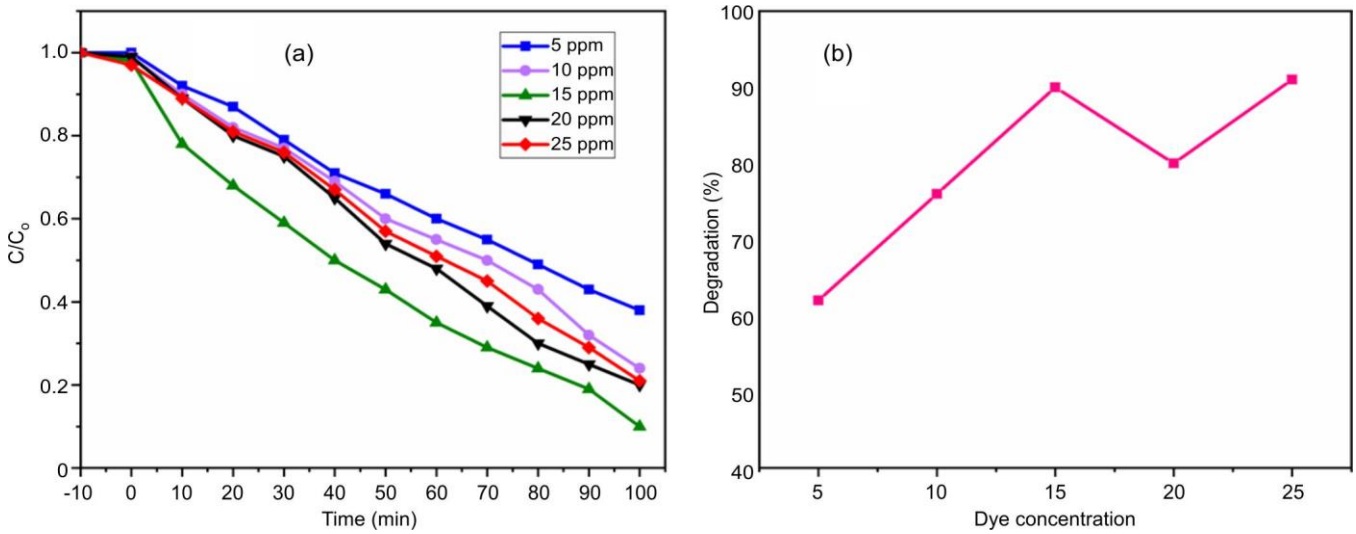

Fig. 9. (a) Impact of initial dye concentration on MG dye, (b) % degradation at different conc. of dye

sites under increased dye loading. Maximum degradation (~98%) is achieved at 15 ppm within 100 min, suggesting optimal interaction between dye molecules and the catalyst surface. Further increase in concentration (20 and 25 ppm) leads to a slight decline in degradation efficiency, likely due to saturation of active sites and reduced light penetration caused by increased solution opacity, which limits reactive species generation. The percentage degradation profile (Fig. 9b) confirms this trend, identifying 15 ppm as the optimum concentration for efficient photocatalytic degradation.

Effect of catalyst: The influence of catalyst dosage on photocatalytic degradation demonstrates that increasing the amount of CuO NPs improves efficiency up to an optimum level. As shown in Fig. 10a, a faster decrease in dye concentration is observed when the dosage is increased from 0.05 to 0.15 g/L, indicating the availability of more active sites and enhanced reaction rates. The maximum degradation (~98%) is achieved at 0.15 g L^{-1}, where the catalyst exhibits optimal performance. However, further increasing the dosage to 0.20 and 0.25 g L^{-1} does not enhance the degradation efficiency; instead, a slight decline is observed. This reduction can be attributed to particle agglomeration and increased solution turbidity, which limit light penetration and decrease photocatalytic activity. The percentage degradation plot in Fig. 10b further confirms that 0.15 g L^{-1} is the optimum catalyst dosage for effective dye removal.

Mechanism of photocatalytic degradation: Under light irradiation, CuO NPs absorb photons and generate electron–hole pairs. The photogenerated holes (h^+) react with adsorbed water or hydroxide ions to form hydroxyl radicals ($^\bullet OH$), while the excited electrons (e^-) reduce dissolved oxygen to produce superoxide radicals ($^\bullet O_2^-$). These reactive species attack the conjugated dye structure, leading to ring opening, cleavage of functional groups and eventual mineralisation. Phytochemical residues from the plant-mediated synthesis may enhance charge separation by acting as surface modifiers, thereby increasing the lifetime of reactive species and improving photocatalytic efficiency [32]. The degradation behaviour aligns with previous studies reporting effective visible-light driven photocatalysis of malachite green using green-synthesised CuO NPs [33], highlighting the role of biogenic surface functionalisation and nanoscale properties in efficient dye removal. The findings indicate that plant-mediated CuO NPs serve as effective and eco-friendly photocatalysts for wastewater treatment applications.

$$\text{CuO NPs} + \text{Visible light} \rightarrow \text{CuO NPs}\,(e^- + h^+) \quad (4)$$

$$\text{CuO NPs}\,(h^+) + H_2O \rightarrow H^+ + {}^\bullet OH \quad (5)$$

$$\text{CuO NPs}\,(h^+) + HO^\bullet \rightarrow {}^\bullet OH \quad (6)$$

$$\text{CuO NPs}\,(e^-) + O_2 \rightarrow {}^\bullet O_2^- \quad (7)$$

$${}^\bullet O_2^- + H^+ \rightarrow {}^\bullet HO_2 \quad (8)$$

$${}^\bullet HO_2 + e^- \rightarrow {}^\bullet OH \quad (9)$$

$${}^\bullet OH + \text{Pollutants} \rightarrow H_2O + CO_2 \quad (10)$$

Conclusion

In present work, copper oxide nanoparticles (CuO NPs) were successfully synthesised *via* an eco-friendly route using *S. aculeata* (Dhaincha) leaf extract as a natural reducing and stabilising agent. XRD analysis confirmed the formation of crystalline monoclinic CuO with an average crystallite size of 22.6 nm, while UV-Vis diffuse reflectance studies indicated a band gap of 2.7 eV. BET analysis revealed a Type IV isotherm with a hysteresis loop, indicating a mesoporous structure with a high surface area of 89.7 m^2 g^{-1}. FESEM images showed agglomerated, irregular particles with rough surfaces and EDS confirmed the presence of copper and oxygen, indicating high purity. Thermogravimetric analysis demonstrated negligible weight loss beyond 400 °C, confirming good thermal stability, while FTIR analysis verified the involvement of phytochemicals in nanoparticle formation and stabilisation. The synthesised CuO NPs exhibited excellent photocatalytic activity, achieving 98% degradation of malachite green dye within 100 min under visible light irradiation. These findings demonstrate that *S. aculeata* leaf extract is an effective and sustainable biogenic resource for producing high-quality CuO NPs with promising applications in environmental remediation.

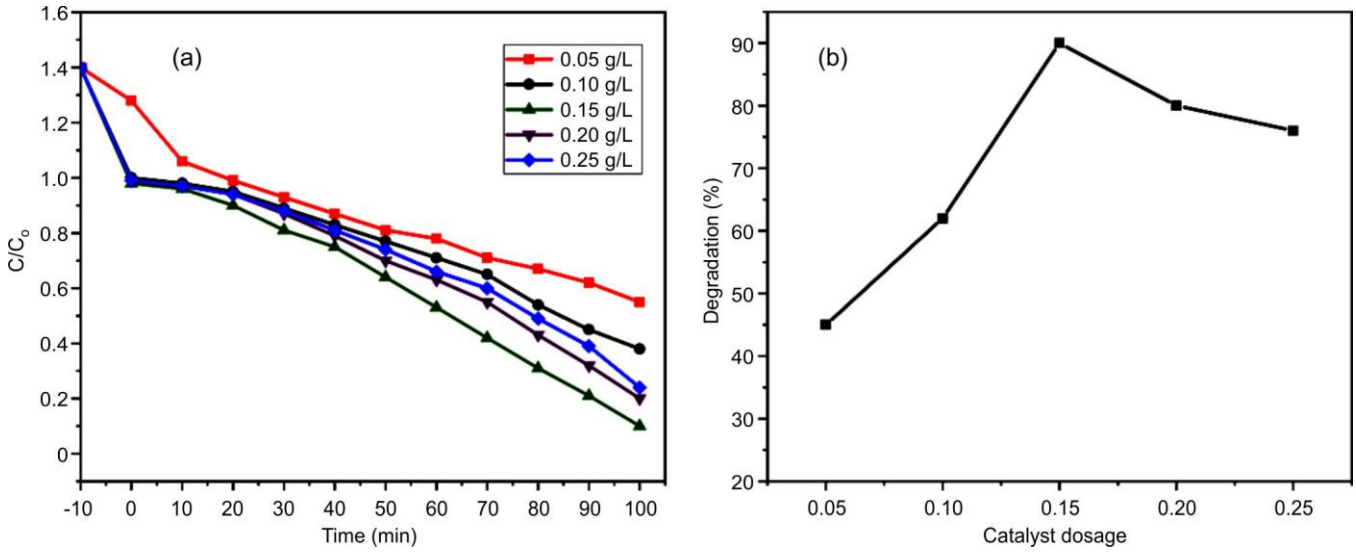

Fig. 10. (a) Effect of catalyst dosage on the degradation of MG dye, (b) % degradation at different catalyst dosage

CONFLICT OF INTEREST

The authors declare that there is no conflict of interests regarding the publication of this article.

DECLARATION OF AI-ASSISTED TECHNOLOGIES

During the preparation of this manuscript, the authors used an AI-assisted tool(s) to improve the language. The authors reviewed and edited the content and take full responsibility for the published work.

REFERENCES

1. A.N. Al-Thani, A.G. Jan, M. Abbas, M. Geetha and K.K. Sadasivuni, *Life Sci.*, **352**, 122899 (2024); https://doi.org/10.1016/j.lfs.2024.122899
2. K. Ali, S. Dwivedi, A. Azam, Q. Saquib, A.A. Alkhedhairy, M.S. Al-Said, and J. Musarrat, *J. Colloid Interface Sci.*, **472**, 145 (2016); https://doi.org/10.1016/j.jcis.2016.03.021
3. I. Khan, K. Saeed and I. Khan, *Arab. J. Chem.*, **12**, 908 (2019); https://doi.org/10.1016/j.arabjc.2017.05.011
4. M. Su, Y. Zhong, J. Xiang, Y. Chen, N. Liu and J. Zhang, *J. Hazard. Mater.*, **455**, 131493 (2024); https://doi.org/10.1016/j.jhazmat.2023.131493
5. K. Sayadi, A. Rahdar, M.R. Hajinezhad, S. Nikazar and M.A.B.H. Susan, *J. Mol. Struct.*, **1202**, 127296 (2020); https://doi.org/10.1016/j.molstruc.2019.127296
6. M.Y. Al-Darwesh, S.S. Ibrahim and M.A. Mohammed, *Results Chem.*, **7**, 101368 (2024); https://doi.org/10.1016/j.rechem.2024.101368
7. Z. Villagrán, L.M. Anaya-Esparza, C.A. Velázquez-Carriles, J.M. Silva-Jara, J.M. Ruvalcaba-Gómez, E.F. Aurora-Vigo, E. Rodríguez-Lafitte, N. Rodríguez-Barajas, I. Balderas-León and F. Martínez-Esquivias, *Resources*, **13**, 70 (2024); https://doi.org/10.3390/resources13060070
8. F. Ulaş, E. Yüksel, D. Dinçer, A. Dababat and M. İmren, *Sustainability*, **17**, 4152 (2025); https://doi.org/10.3390/su17094152
9. N. Anwar, M. Shah, S. Saleem and H. Rahman, *Bull. Chem. Soc. Ethiop.*, **32**, 469 (2018); https://doi.org/10.4314/bcse.v32i3.6
10. N. Rani, P. Singh, S. Kumar, P. Kumar, V. Bhankar and K. Kumar, *Mater. Res. Bull.*, **163**, 112233 (2023); https://doi.org/10.1016/j.materresbull.2023.112233
11. P. Singh, Y.J. Kim, D. Zhang and D.C. Yang, *Trends Biotechnol.*, **34**, 588 (2016); https://doi.org/10.1016/j.tibtech.2016.02.006
12. K.A. de Jesus, G.C. de Assis, R.J. de Oliveira, J.A.S. Costa, C.M.P. da Silva, M. Bilal, H.M.N. Iqbal, L.F.R. Ferreira and R.T. Figueiredo, *Environ. Technol. Innov.*, **24**, 101851 (2021); https://doi.org/10.1016/j.eti.2021.101851
13. M. Pourmadadi, R. Holghoomi, A. Shamsabadipour, R. Maleki-Baladi, A. Rahdar and S. Pandey, *Plant Nano Biol.*, **8**, 100070 (2024); https://doi.org/10.1016/j.plana.2024.100070
14. R. Shaik, A. Buggana, V. Thalari, S. Rano, B. Kedharnath and N. Golla, *Int. J. Nanodimens.*, **16**, 1 (2025); https://doi.org/10.57647/j.ijnd.2025.1601.05
15. Z. Duan, G. Ma and W. Zhang, *Bull. Korean Chem. Soc.*, **33**, 4003 (2012); https://doi.org/10.5012/bkcs.2012.33.12.4003
16. M. Thiruvengadam, I.-M. Chung, T. Gomathi, M.A. Ansari, V. Gopiesh Khanna, V. Babu and G. Rajakumar, *Bioprocess Biosyst. Eng.*, **42**, 1769 (2019); https://doi.org/10.1007/s00449-019-02173-y
17. M. Barbouchi, B. Benzidia, K. Elamrani, M. Sabiri, M. El Idrissi and M. Choukrad, *Kuwait J. Sci.*, **51**, 100287 (2024); https://doi.org/10.1016/j.kjs.2024.100287
18. E. Mathe, L. Sethoga, S. Mapfumari, O. Adeniran, P. Mokgotho, J. Shai and S. Gololo, *Life*, **14**, 1375 (2024); https://doi.org/10.3390/life14111375
19. M.K. Ghosh, S. Sahu, I. Gupta and T.K. Ghorai, *RSC Adv.*, **10**, 22027 (2020); https://doi.org/10.1039/D0RA03186K
20. M. Rangasamy, S.K. Gopal, A. Indhumathi, S. Loganathan, S. Manikandan and R. Naresh, *J. Pharm. Res. Int.*, **35**, 9 (2023); https://doi.org/10.9734/jpri/2023/v35i77335
21. A. Matei, G. Craciun, C. Romanitan, C. Pachiu and V. Tucureanu, *Eng. Proc.*, **37**, 54 (2023); https://doi.org/10.3390/ECP2023-14629
22. I.H. Shah, M. Ashraf, I.A. Sabir, M.A. Manzoor, M.S. Malik, S. Gulzar, F. Ashraf, J. Iqbal, Q. Niu and Y. Zhang, *J. Mol. Struct.*, **1259**, 132696 (2022); https://doi.org/10.1016/j.molstruc.2022.132696
23. Y.-P. Liang, Y.-B. Chan, M. Aminuzzaman, M. Shahinuzzaman, S. Djearamane, K. Thiagarajah, S.-Y. Leong, L.-S. Wong and L.-H. Tey, *Catalysts*, **15**, 275 (2025); https://doi.org/10.3390/catal15030275
24. I.H. Bhuiyan, S.P. Moulick, M.R. Islam, M. Sahadat Hossain, S.S. Dey, S.A. Chhanda, F. Ahmed, M.F. Ahmed and T. Muslim, *ChemistrySelect*, **10**, e03202 (2025); https://doi.org/10.1002/slct.202503202
25. A. Atri, M. Echabaane, A. Bouzidi, I. Harabi, B.M. Soucase and R.B. Chaâbane, *Heliyon*, **9**, e13484 (2023); https://doi.org/10.1016/j.heliyon.2023.e13484
26. M.I. Said, A.A. Othman and E.M. Abd elhakeem, *RSC Adv.*, **11**, 37801 (2021); https://doi.org/10.1039/D1RA04780A
27. H.K. Abid, A.B. Siddique, A. Abbas, M.A. Shaheen, A. Ali, M. Fatima, A. Shami, M.A. Alrayyani, F.A. Al-Joufi and M.A. Assiri, *Nanoscale Adv.*, **7**, 6145 (2025); https://doi.org/10.1039/D5NA00583C
28. C.A. Magaña-Chavez, J.A. Villegas-Fuentes, O.J. Nava, A.R. Vilchis-Nestor and P.A. Luque, *J. Mater. Sci. Mater. Electron.*, **36**, 1728 (2025); https://doi.org/10.1007/s10854-025-15811-x
29. A.H. Anchani, A.H. Abishini and T. Ashokkumar, *Discover Biotechnol.*, **1**, 4 (2024); https://doi.org/10.1007/s44340-024-00004-9
30. M. Batool and N. Mehboob, *Arch. Nanomed.*, **1**, 29 (2018); https://doi.org/10.32474/ANOAJ.2018.01.000108
31. L.T. Tai, N.M. Dat, N.T.H. Nam, H. An, L.M. Huong, C.Q. Cong, N.D. Hai, M.T. Phong and N.H. Hieu, *Optical Mater.*, **136**, 113489 (2023); https://doi.org/10.1016/j.optmat.2023.113489
32. L.T. Tai, N.M. Dat, N.T.H. Nam, H. An, L.M. Huong, C.Q. Cong, N.D. Hai, M.T. Phong and N.H. Hieu, *Opt. Mater.*, **136**, 113489 (2023); https://doi.org/10.1016/j.optmat.2023.113489
33. S. Aroob, S.A.C. Carabineiro, M.B. Taj, I. Bibi, A. Raheel, T. Javed, R. Yahya, W. Alelwani, F. Verpoort, K. Kamwilaisak, S. Al-Farraj and M. Sillanpää, *Catalysts*, **13**, 502 (2023); https://doi.org/10.3390/catal13030502